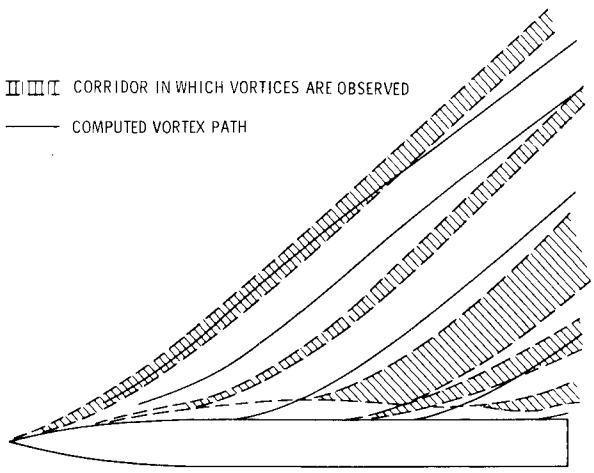

Fig. 4 Comparison of observed and computed vortex paths. $\alpha = 45°$; $M = 0.5$.

different experimental curves are shown, each corresponding to a different nose roll angle. The calculated side forces are of the correct size and occur at the appropriate range in angle of attack. For Mach numbers greater than 0.9, the side force is observed experimentally to decrease, while the predicted value of the side force remains unchanged. In Fig. 4, the predicted vortex paths are compared to those observed from schlieren pictures indicating a qualitative agreement between the predicted and observed structure of the vortex wake.

The vortex strengths predicted by the current model in the above example are typically 30% larger than those measured by Thomson and Morrison.[8]

Comparison with data obtained by G. Pick[9] indicates that the computed normal force coefficients correctly reflect the experimentally determined changes in the normal force caused by the nose bluntness, with the most satisfactory results occurring at subsonic Mach numbers. However, the decreasing yaw force coefficient which is seen to accompany increasing nose bluntness is not predicted by the current model. A more comprehensive comparison between the described model and experimental results is given in Ref. 6.

Conclusions

The model described correctly predicts normal forces and gives a good approximation of yawing forces on slender bodies at subsonic Mach numbers. For these conditions, a more accurate determination of the side forces would require an analysis which includes model and flowfield nonuniformities, since, as can be seen from Fig. 3, these parameters have a great effect on yawing force. The current model could be most improved by extending the Mach number range over which it is valid and by improving its ability to account for the effect of nose bluntness in predicting yaw forces.

References

[1] Jorgensen, L. H., "Prediction of Static Aerodynamic Characteristics for Space-Shuttle-Like and Other Bodies at Angles of Attack Varying from 0° to 180°," TN D-6996, Jan. 1973, NASA.

[2] Allen, H. J., "Estimation of Forces and Moments on Inclined Bodies of Revolution of High Fineness Ratio," RM A9126, 1949, NACA.

[3] Kelly, H. R., "Estimation of Normal Force and Pitching Moment Coefficient for Blunt Based Bodies of Revolution at Large Angles of Attack," *Journal of the Aerospace Sciences*, Vol. 21, No. 8, Aug. 1954.

[4] Bryson, A. E., "Symmetric Vortex Separation on Circular Cylinders and Cones," *Journal of Applied Mechanics*, Vol. 26, No. 4, Dec. 1959, pp. 643–648.

[5] Schindel, L. H., "Effects of Vortex Separation on the Lift Distribution of Bodies of Elliptical Cross Section," *Journal of Aircraft*, Vol. 6, No. 6, June 1969, pp. 537–542.

[6] Wardlaw, A. B., Jr., "Prediction of Normal Force, Pitching Moment, and Yawing Force on Bodies of Revolution at Angles of Attack up to 50 Degrees Using a Concentrated Vortex Flow-Field Model," NOLTR 73-209, Oct. 1973, Naval Ordnance Lab., Silver Spring, Md.

[7] Schindel, L. H., "Effects of Vortex Separation on Lifting Bodies of Elliptic Cross Section," TR 118, Sept. 1965, MIT Aerophysics Lab., Cambridge, Mass.

[8] Thomson, K. D. and Morrison, D. F., "The Spacing, Position and Strengths of Vortices in the Wake of Slender Cylindrical Bodies at Large Incidence," *Journal of Fluid Mechanics*, Vol. 50, Pt. 4, 1971, pp. 751–783.

[9] Pick, G., "Side Forces on Ogive-Cylinder Bodies at High Angles of Attack in Transonic Flow," *Journal of Spacecraft and Rockets*, Vol. 9, No. 6, June 1972, pp. 389–390.

Radiation-Gas Dynamic Shock Layer Coupling

CARL D. ENGEL* AND RICHARD C. FARMER†
Louisiana State University, Baton Rouge, La.

Nomenclature

E_2 = exponential integral
P_δ = postshock pressure
U_∞ = freestream velocity
q_R = surface radiative heat flux
$q_{R,I}$ = isothermal shock layer flux for postshock conditions
Γ = radiative cooling parameter $\Gamma = 2q_{R,I}(\frac{1}{2}\rho_\infty U_\infty{}^3)$
Δ = ratio of radiationless shock detachment distance to nose radius
δ = ratio of shock detachment distance to nose radius
$\bar{\rho}$ = density ratio across shock ρ_∞/ρ_δ

Subscripts

δ = postshock
∞ = freestream

Introduction

THE effects of radiation losses on the shock layer during hypersonic flight has been of interest for several years. Early work was characterized by examination of limiting solutions of the thin shock layer equations for optically thin and thick radiating gases to provide an overview of radiation-gas dynamic coupling.[1] More recent work has concentrated on obtaining detailed shock layer solutions which include the effects of nongray continuum and line radiation, viscous dissipation and ablation.[2–5] These detailed solutions were obtained for a variety of specific flight conditions. The purpose herein is to present detailed stagnation line shock layer results for a wide range of flight conditions which can be compared with the earlier work and provide a new overview of radiation-gas dynamic coupling within a shock layer. Only nonablating bodies are considered in this Note.

The stagnation region of a viscous radiating shock layer was modeled in Ref. 5 and is the basis for the results presented herein. This model consist of the viscous stagnation line

Received December 3, 1973. The authors are grateful for support from NASA Grant NGR 19-001-059 during the course of this investigation.

Index categories: Radiatively Coupled Flows and Heat Transfer; Supersonic and Hypersonic Flow; Radiation and Radiative Heat Transfer.

* Research Associate, Chemical Engineering Department; now Research Specialist, REMTECH Inc., Huntsville, Ala. Associate Member AIAA.

† Professor of Chemical Engineering.

continuity, momentum, and energy equations for a thin shock layer. The radiative flux divergence term in the energy equation was computed using a one-dimensional thin slab model. Nongray continuum and line radiation from N and O and continuum radiation from N_2 and O_2 were included. Air equilibrium thermodynamic and transport properties were obtained by the method of Hansen.[6] An implicit finite-difference method together with under-relaxation successive-substitution was used to solve the momentum and energy equations.

Results

The shock wave location is a boundary condition for the thin shock layer equations. Mathematically this boundary condition is known as a free boundary and is determined by the solution of the equations in the bounded region. For the problem under investigation, the shock standoff distance is determined by the radiation-gas dynamic coupling which occurs in the shock layer.

Stagnation line solutions were obtained for freestream velocities between 36,000 and 58,000 fps at postshock pressure levels of $P_\delta = 1.0$, 0.50, 0.10, and 0.01 atm for a wall temperature of 3450°K and no mass injection. The nondimensional standoff distances resulting from these calculations are shown in Fig. 1 as a function of density ratio across the shock. Along with the computed results are plots of two commonly used correlation equations which were developed to predict nonradiatively coupled standoff distances. It is noted that the correlation of Inouye[7] predicts larger standoff distances than any obtained by the present method; however, the correlation presented in Ref. 8 agrees to within 3% with the four points for 36,000 fps where the effects of radiative coupling are small. Thus the correlation from Ref. 8 provides a quite reasonable estimate of the nonradiatively coupled standoff distance.

The present results shown in Fig. 1 indicate some additional interesting processes. Most obviously, the standoff distance is a strong function of the postshock pressure. The constant pressure lines show a double value for δ at constant $\bar{\rho}$. This effect, which occurs at the higher velocities, is a natural result of air thermodynamics being used to solve the Rankine-Hugoniot equations. It is also noted that the turn in the constant pressure line gets sharper with decreasing pressure until the standoff distance becomes double valued for the pressure $P_\delta = 0.01$ atm.

A measure of the radiative-gas dynamic coupling effects on the standoff distance can be shown by observing the actual standoff distance, δ, divided by the radiationless standoff distance, Δ, obtained from Ref. 8. Accordingly, the deviation from the radiationless shock layer distance is expressed as

$$\delta/\Delta = \delta[1 + (8\bar{\rho}/3)]^{1/2}/\bar{\rho} \qquad (1)$$

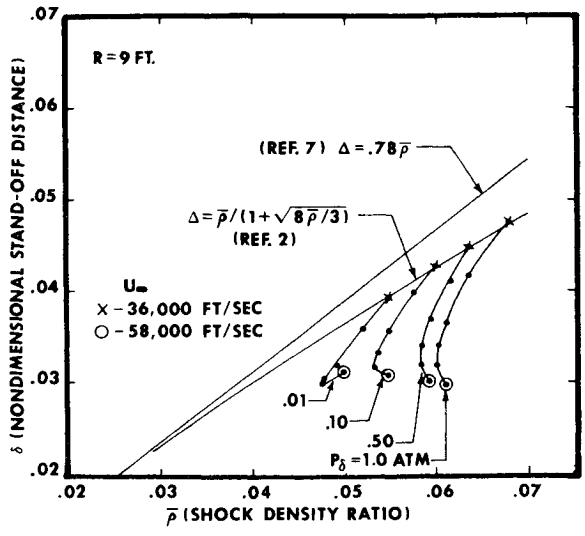

Fig. 1 Radiative coupled shock standoff distances.

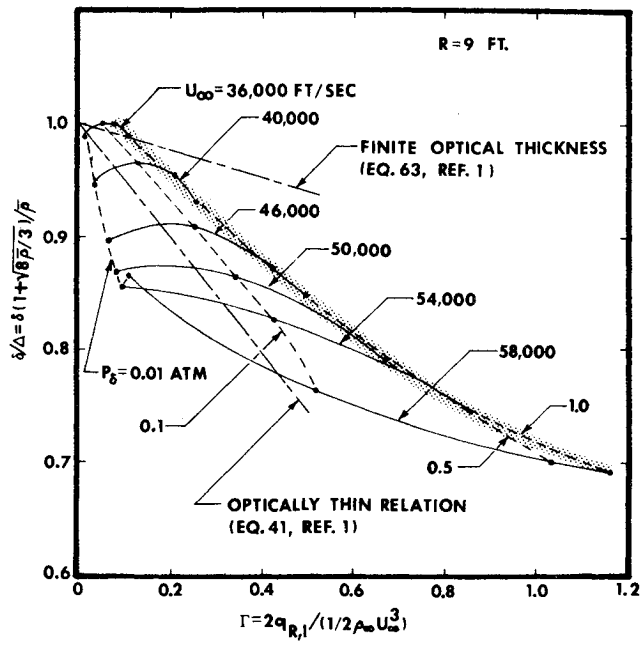

Fig. 2 Radiative cooling effects on standoff distances.

Figure 2 shows the effects of radiation coupling on the standoff distance as a function of the radiative cooling parameter, Γ. The cooling parameter was computed using the same line and continuum radiation model used in the flowfield solution and is based on the radiationless standoff distance. The results indicate that the ratio δ/Δ at constant P_δ varies linearly with Γ for small values of Γ. It is noted that there is an apparent translation at $\delta/\Delta = 1.0$ for different pressure levels. This is attributed to the representation of Δ with Eq. (1) rather than using the actual radiationless standoff distance.

A comparison of the present results with previous estimates of Goulard[1] shown in Fig. 2 provides additional insight into the radiation coupling effects. Goulard formulated the stagnation line problem with a simple inviscid flowfield model and a gray gas radiation model. The effects of radiation-gas dynamic coupling on the standoff distance were studied using a perturbation scheme for small values of Γ. Results were obtained for optically thin and finite thickness limits. The finite optically thickness results, Eq. (63) of Ref. 1

$$\delta/\Delta = 1 - \tfrac{1}{2}\Gamma E_2(\eta_\Delta/2) \qquad (2)$$

is in terms of the exponential integral dependence on $\eta_\Delta = \rho_\delta K_\delta \Delta$. This parameter is a product of the postshock density, frequency averaged mass absorption coefficient and Δ. The optically thin results are identical to the preceding expression with the exception that the exponential integral, E_2, is equal to one.

Utilizing the finite optical thickness results, Goulard found a minimum value of δ/Δ for horizontal flight which corresponded to a value of $\eta_\Delta = \frac{4}{3}$. Results for $\eta_\Delta = \frac{4}{3}$ are shown in Fig. 2 which tend to underpredict the radiative cooling effects. The optically thin results of the simple model presented in Fig. 2 also underpredict the radiative cooling effects. It should be emphasized that Goulard's analysis is valid only for $\Gamma \ll 1$. The trends shown by the simplified model are in agreement with the present results. That is, an increase in optical thickness corresponding to increasing postshock pressure trends to decrease the radiative cooling effect of reducing the shock standoff distance.

The results presented in Fig. 2 of constant postshock pressure lines approximate horizontal flight while the lines of constant velocity approximate vertical flight. The set of constant velocity curves appear to form a surface which has an asymptotic limit on the optically thick side. Further, the asymptotic appears nearly linear for values of Γ less than 0.5 and corresponds to the $P_\delta = 1.0$ and 0.5 atm results. For larger values of Γ a minimum

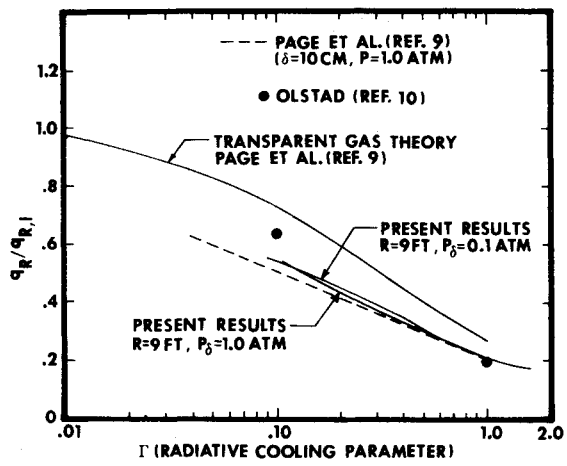

Fig. 3 Radiative heating vs radiative cooling parameter results.

value in the asymptote for δ/Δ appears to be approached. It is anticipated that for flight velocities higher than approximately 58,000 fps precursor radiation will become significant resulting in an increase in δ/Δ, since a portion of the energy lost by radiation through the shock wave which reduces the standoff distance will be absorbed by the oncoming gas and returned to the shock layer.

In the case of vertical entry (i.e., constant U_∞), the maximum collapse of the shock layer occurs along a line formed by conditions for $P_\delta \geqq 0.5$ atm. This contradicts Goulard's conclusion that the minimum δ/Δ would occur in the early part of atmospheric penetration.

In the case of near horizontal flight (i.e., constant P_δ) of a constant accelerating vehicle, radiationless shock layer thickness would occur followed by a linearly decreasing thickness. Further acceleration would result in a minimum and then increased thickness. This is in qualitative agreement with Goulard's conclusions.

The effects of radiation-gas dynamic coupling are also reflected in the radiative heating to the surface. Radiative heating rates from the present analysis are compared in nondimensional form with results of other investigators in Fig. 3. The present results correlate quite well with the radiative cooling parameter, Γ, and lie between the results of two inviscid shock layer analyses.[9,10] All of the shock layer results presented in Fig. 3 lie below the transparent gas theory results of Ref. 9. As pointed out by Page[9] the transparent theory is inadequate for predicting heating since the true optical properties of the shock layer are not uniformly optically thin. This result is certainly in accord with the results given in Fig. 2. The important point illustrated in Fig. 3 is that the radiative heating can be correlated with a single parameter, Γ, with little approximation and that both viscous and inviscid analyses yield similar results.

In conclusion, the radiation-gas dynamic coupling effect on the radiative heating can be related to the single parameter, Γ, whereas the effect on the shock layer thickness is not a simple function of this parameter.

References

[1] Goulard, R., "Preliminary Estimates of Radiative Transfer Effects on Detached Shock Layers," *AIAA Journal*, Vol. 2, No. 3, March 1964, pp. 494–502.

[2] Wilson, K. H., "Stagnation Point Analysis of Coupled Viscous-Radiating Flow with Massive Blowing," CR-1548, June 1970, NASA.

[3] Rigdon, W. S., Dirling, R. B., Jr., and Thomas, M., "Stagnation Point Heat Transfer During Hypervelocity Atmospheric Entry," CR-1462, Feb. 1970, NASA.

[4] Smith, G. L., Suttles, J. T., and Sullivan, E. M., "Viscous Radiating Flowfield on an Ablating Blunt Body," AIAA Paper 70-218, New York, 1970.

[5] Engel, C. D., Farmer, R. C., and Pike, R. W., "Ablation and Radiation Coupled Viscous Hypersonic Shock Layers," *AIAA Journal*, Vol. 11, No. 8, Aug. 1973, pp. 1174–1181.

[6] Hansen, C. F., "Approximations for Thermodynamic Properties of High Temperature Air," TR R-50, 1959, NASA.

[7] Inouye, M., "Blunt Body Solutions for Spheres and Ellipsoids in Equilibrium Gas Mixtures," TN D-2780, 1965, NASA.

[8] Hayes, W. D. and Probstein, R. F., *Hypersonic Flow Theory*, 2nd ed., Academic Press, New York, 1966.

[9] Page, W. A., Compton, D. L., Borucki, W. J., Ciffone, D. L., and Cooper, D. M., "Radiative Transport in Inviscid Nonadiabatic Stagnation-Region Shock Layers," *AIAA Progress in Astronautics and Aeronautics: Thermal Design Principles of Spacecraft and Entry Bodies*, Vol. 21, edited by Jerry T. Bevans, Academic Press, New York, 1969, pp. 75–114.

[10] Olstad, W. B., "Correlations for Stagnation-Point Radiative Heat Transfer," *AIAA Journal*, Vol. 7, No. 1, Jan. 1969, pp. 170–172.

Laminar Viscous-Inviscid Interactions at Transonic Speeds

DONALD J. COLLINS*
Jet Propulsion Laboratory, Pasadena, Calif.

Introduction

THE interaction between the boundary layer which forms on an aerodynamic surface and the inviscid outer flowfield is most pronounced at transonic speeds where the nature of the mixed supersonic and subsonic inviscid flowfield is often determined by the viscous portions of the flow. The early measurements by Ackeret et al.[1] and by Liepmann et al.[2] have explored some of the effects of viscosity and its influence on the over-all development of a transonic flowfield. More recently, the measurements reported by Alber et al.[3] have examined some of the details of a transonic turbulent boundary layer which separates either in the shock-interaction or in the pressure-gradient mode. In each of these investigations, it has been clear that a strong interaction exists between the viscous and the inviscid flows, and as a consequence the boundary layer cannot be treated theoretically as a small perturbation to the outer flow, but must be closely coupled with the outer flow, and must be solved simultaneously. The present Note will discuss some aspects of the laminar viscous-inviscid interaction at transonic speeds by examining data obtained on a 6% thick biconvex circular-arc airfoil and comparing the results with the predictions of Klineberg and Steger.[4]

Experimental Technique

The present experiments have been performed in the Jet Propulsion Lab. 20-in. wind tunnel at Mach numbers $0.6 \leqq M_\infty \leqq 0.915$ and Reynolds numbers $3.9 \times 10^4 \leqq Re \leqq 1.2 \times 10^6$, based on chord. Details of the model construction are given by Collins[5] and experimental details are given in Collins and Krupp.[6]

Received December 10, 1973; revision received February 28, 1974. This Note presents the results of one phase of research carried out at the Jet Propulsion Laboratory, under Contract NAS7-100, sponsored by NASA. The author would like to acknowledge the many valuable interactions with J. Krupp and J. Cole during the course of this research. Their contributions to this work have been both timely and numerous. Furthermore, the author wishes to acknowledge the excellent assistance of C. Nussey and R. Morrow and the entire Jet Propulsion Wind-Tunnel Staff in the performance of the experiments.

Index categories: Subsonic and Transonic Flow; Jets, Wakes, and Viscous-Inviscid Interactions.

* Senior Scientist, Physics Section. Member AIAA.